Chemical Science

ROYAL SOCIETY OF CHEMISTRY

PERSPECTIVE

View Article Online
View Journal | View Issue

Check for updates

Cite this: *Chem. Sci.*, 2024, **15**, 8265

All publication charges for this article have been paid for by the Royal Society of Chemistry

Received 3rd March 2024
Accepted 6th May 2024

DOI: 10.1039/d4sc01481b

rsc.li/chemical-science

Open Access Article. Published on 07 maggio 2024. Downloaded on 18/04/2026 16:34:18.
This article is licensed under a Creative Commons Attribution-NonCommercial 3.0 Unported Licence.

Quinoxaline-based Y-type acceptors for organic solar cells

Meiling Xie,[ab] Zhixiang Wei *[ab] and Kun Lu *[ab]

Minimizing energy loss plays a critical role in the quest for high-performance organic solar cells (OSCs). However, the origin of large energy loss in OCSs is complicated, involving the strong exciton binding energy of organic semiconductors, nonradiative charge-transfer state decay, defective molecular stacking network, and so on. The recently developed quinoxaline (Qx)-based acceptors have attracted extensive interest due to their low reorganization energy, high structural modification possibilities, and distinctive molecular packing modes, which contribute to reduced energy loss and superior charge generation/transport, thus improving the photovoltaic performance of OSCs. This perspective summarizes the design strategies of Qx-based acceptors (including small-molecule, giant dimeric and polymeric acceptors) and the resulting optoelectronic properties and device performance. In addition, the ternary strategy of introducing Qx-based acceptors as the third component to reduce energy loss is briefly discussed. Finally, some perspectives for the further exploration of Qx-based acceptors toward efficient, stable, and industry-compatible OSCs are proposed.

1. Introduction

Organic solar cells (OSCs) represent a promising photovoltaic technology for multi-scene applications due to their various advantages, such as lightweight, flexibility, and semitransparency.[1–3] Benefiting from a deeper understanding of material design and device engineering, the state-of-the-art single-junction OCSs have achieved power conversion efficiencies (PCEs) of over 19%.[4–7] Specifically, the PCE is determined by three critical parameters, including open-circuit voltage (V_{OC}), short-circuit current density (J_{SC}), and fill factor (FF). However, the inferior V_{OC} of OSCs compared to perovskite and inorganic solar cells, caused by larger energy losses (E_{loss}), is still a major obstacle to further improvement of device performance.[8–10] Therefore, it is necessary to investigate the origin of E_{loss} and to develop effective OSC systems with low E_{loss}.

According to Shockley–Queisser (SQ) limit theory, the E_{loss} in photovoltaic cells could be divided into three parts (Fig. 1a): radiative energy loss above the bandgap (ΔE_1), radiative energy loss below the bandgap (ΔE_2) due to non-step function absorption for practical devices, and nonradiative energy loss (ΔE_3).[11] In addition, ΔE_3 can be calculated from the equation: $\Delta E_3 = -k_B T \ln(EQE_{EL})$, where k_B, T, and EQE_{EL} are the Boltzmann constant, temperature, and external electroluminescence quantum efficiency of the device, respectively.[12] Considering the bandgap dependent ΔE_1 and the negligible ΔE_2 in the emerging non-fullerene acceptor (NFA)-based OSCs, the reduction of E_{loss} is mainly focused on minimizing ΔE_3.[13–16] To this end, chemical modifications of acceptor materials have been widely applied to optimize their electronic structures and aggregation behaviors, resulting in effective hybridization of local exciton (LE) and charge-transfer (CT) states, decreased energetic disorder, and increased photoluminescence quantum yield (PLQY).[17–20] Nevertheless, numerous studies have shown that a better trade-off between V_{OC} and J_{SC} is essential for high-efficiency OSCs.[21–23] Only under the premise of efficient charge generation is the rational pursuit of low E_{loss} conducive to the further development of OSCs to a new milestone, which requires the precise design of organic semiconductors and fine-tuning of the film morphology.

As mentioned above, the significant progress in the PCE of OSCs can largely be attributed to the innovation of NFAs, such as ITIC, Y6, and their derivatives.[24–30] Among them, the efficient Y-series acceptors show unique molecular packing behaviors to form a three-dimensional (3D) stacking network, which enables effective charge transport/collection and low E_{loss} in relevant OSCs.[31,32] Such a distinctive molecular packing is attributed not only to terminal group interactions, but also to the interaction between the central units, highlighting the critical role of central-unit modification in the construction of efficient NFAs. Significantly, the recently developed quinoxaline (Qx)-based acceptors with multiple substitution sites on the central unit have attracted considerable interest because of their reduced energy losses, abundant structural modification possibilities, diverse molecular packing modes, and favorable film

[a]CAS Key Laboratory of Nanosystem and Hierarchical Fabrication, CAS Center for Excellence in Nanoscience, National Center for Nanoscience and Technology, Beijing 100190, China

[b]University of Chinese Academy of Sciences, Beijing 100049, China. E-mail: weizx@nanoctr.cn; lvk@nanoctr.cn

© 2024 The Author(s). Published by the Royal Society of Chemistry

Open Access Article. Published on 07 maggio 2024. Downloaded on 18/04/2026 16:34:18.
This article is licensed under a Creative Commons Attribution-NonCommercial 3.0 Unported Licence.

morphology, showing great potential for achieving a better balance among V_{OC}, J_{SC}, and FF.[33–35] In this perspective, we summarize the molecular design strategies and progress of Qx-based acceptors for OSCs, including small-molecule, giant dimeric, and polymeric acceptors. The development of ternary OSCs with Qx-based acceptors as the third component is then briefly discussed. Finally, several potential directions for further exploration of Qx systems towards efficient and stable OSCs are proposed with the aim of promoting their commercial applications.

2. The development of Qx-based acceptors

In general, Y-series NFAs with an A–DA′D–A framework (where A is an electron-deficient acceptor moiety and D is an electron-rich donor moiety) are composed of a central unit, end groups, and stretched side chains. The Qx moiety and its derivatives, which possess a quinoid resonance effect and additional modification sites, have been introduced to replace the A′ moiety (benzothiadiazole, BT) in Y6 *via* a one- or two-step reaction (Fig. 1b and c), which is beneficial for fine-tuning the optoelectronic properties and intermolecular packing behaviors of acceptors, thus enhancing the photovoltaic performance of relevant OSCs. In 2019, Zhu and co-workers first reported a pair of NFAs, AQx-1 and AQx-2 (Fig. 2), with Qx-containing central units. The AQx-1 based device shows an extremely small highest occupied molecular orbital (HOMO) offset (0.02 eV) and low energy loss (0.52 eV). To balance the trade-off between the V_{OC} and charge generation, AQx-2 was developed by removing the electron-donating methyl substituents in the Qx moiety, resulting in a stronger π–π interaction and a reduced phase separation size when blended with the donor PM6. Due to more balanced charge transport and suppressed recombination, AQx-2-based OSCs deliver a significantly improved PCE of 16.64% (Table 1) compared to AQx-1-based OSCs (13.31%).[33] This is followed by the development of a range of Qx-based acceptors with innovative structures, resulting in a champion PCE of over 19.5% and an E_{loss} of 0.518 eV for binary OSCs.[36] In this section, we discuss the progress of Qx-based acceptors for efficient OSCs from a molecular design perspective, focusing on the effects of conjugated extension, halogenation, and side-chain modification in small-molecule acceptors (SMAs). Furthermore, the recent advances in Qx-based giant dimeric and polymeric acceptors are concisely summarized. The ternary strategy of incorporating Qx-based acceptors as the third component to reduce E_{loss} is also presented.

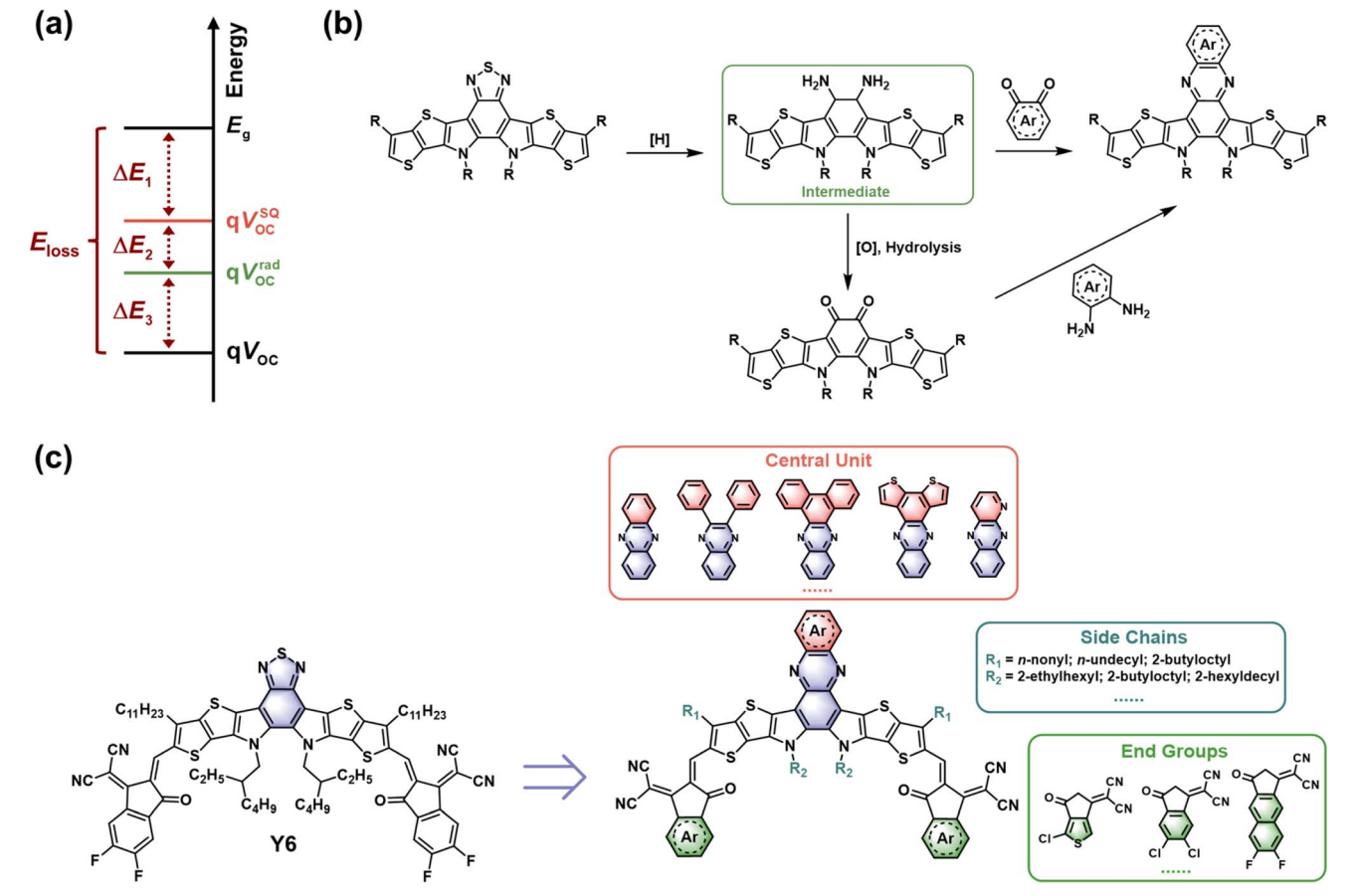

Fig. 1 (a) Energy loss diagram of photovoltaic cells. (b) Typical synthetic routes of Qx central units. (c) Schematic diagram of the structural modification of Qx-based acceptors.

© 2024 The Author(s). Published by the Royal Society of Chemistry

Open Access Article. Published on 07 maggio 2024. Downloaded on 18/04/2026 16:34:18.
This article is licensed under a Creative Commons Attribution-NonCommercial 3.0 Unported Licence.

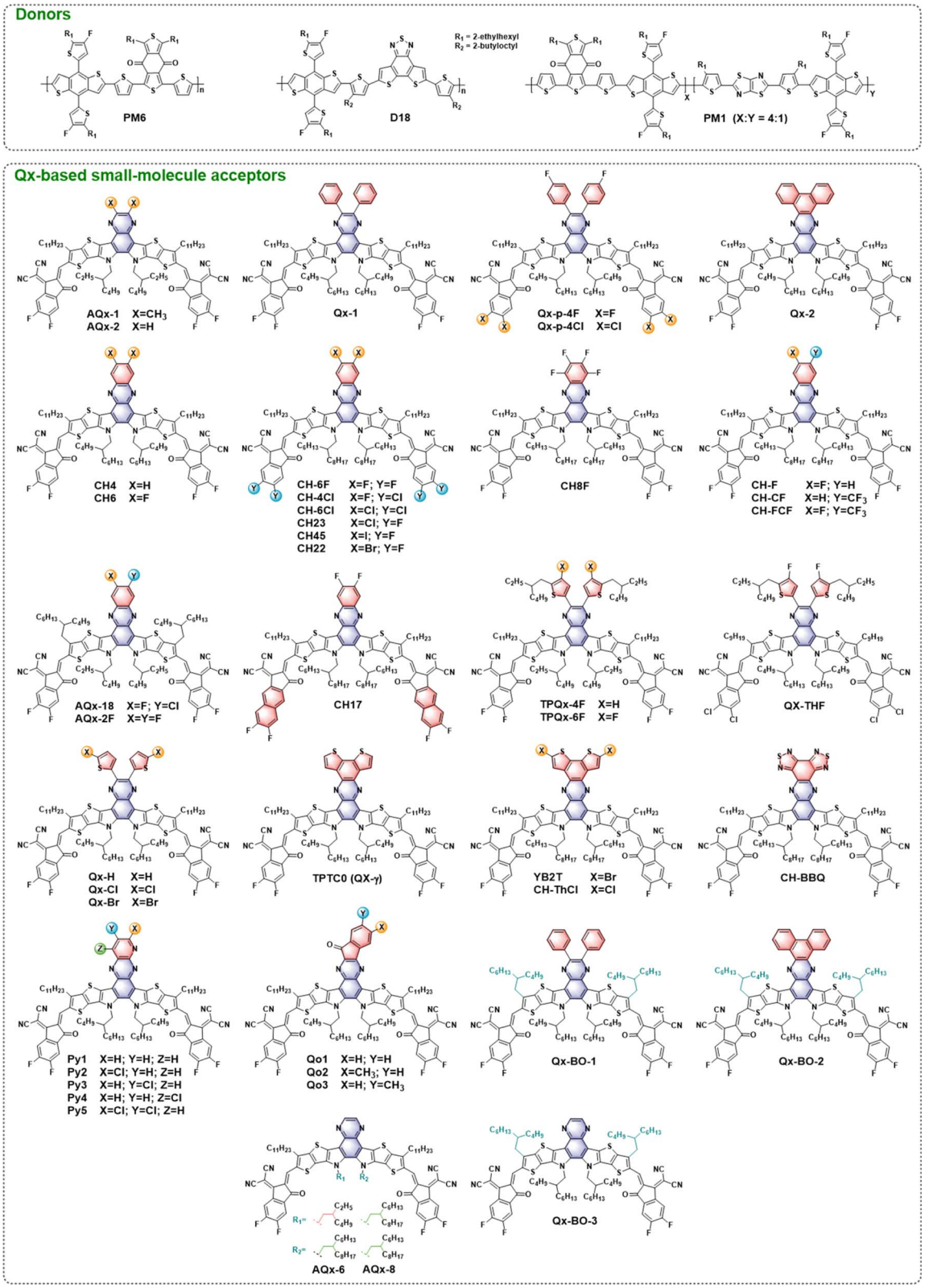

Fig. 2 Chemical structures of donors and Qx-based small-molecule acceptors mentioned in this perspective.

2.1 Qx-based small-molecule acceptors

2.1.1 Conjugated extension and halogenation of Qx-based SMAs. The π-conjugated extension and halogenation of the central unit are feasible strategies to tune the energy levels, absorption, molecular stacking, and crystallinity of acceptors. Significantly, various aromatic and heteroaromatic rings have

Open Access Article. Published on 07 maggio 2024. Downloaded on 18/04/2026 16:34:18.
This article is licensed under a Creative Commons Attribution-NonCommercial 3.0 Unported Licence.

Table 1 The photovoltaic parameters of Qx-based small-molecule acceptors

Acceptor	HOMO/LUMO [eV]	E_g^{opt} [eV]	Donor	V_{OC} [V]	J_{SC} [mA cm^{-2}]	FF [%]	PCE [%]	E_{loss} [eV]	ΔE_3 [eV]	Ref.
AQx-1	−5.59/−3.85	1.37	PM6	0.89	22.18	67.14	13.31	0.52	0.23	33
AQx-2	−5.62/−3.88	1.36	PM6	0.86	25.38	76.25	16.64	0.54	0.24	33
Qx-1	−5.58/−3.98	1.36	PM6	0.911	26.1	75.5	17.9	0.508	0.214	34
Qx-2	−5.54/−3.86	1.36	PM6	0.934	26.5	73.7	18.2	0.482	0.190	34
Qx-*o*-4F	−5.73/−3.92	1.44	PM6	0.928	23.64	75.46	16.55	0.522	0.202	23
Qx-*m*-4F	−5.69/−3.82	1.45	PM6	0.898	24.55	76.89	16.95	0.549	0.229	23
Qx-*p*-4F	−5.76/−3.91	1.47	PM6	0.877	24.89	79.46	17.34	0.560	0.246	23
Qx-*p*-4Cl	−5.65/−3.96	1.41	PM6	0.879	25.63	80.17	18.06	0.535	0.225	23
CH4	−5.64/−3.83	1.37	PM6	0.888	26.11	71.1	16.49	0.51	0.21	22
CH6	−5.68/−3.85	1.40	PM6	0.875	26.62	78.4	18.33	0.53	0.23	22
CH-6F	−5.70/−3.85	1.41	PM6	0.872	25.31	75.99	16.77	0.557	0.232	37
CH-4Cl	−5.74/−3.91	1.39	PM6	0.872	26.50	76.68	17.72	0.537	0.224	37
CH-6Cl	−5.79/−3.97	1.36	PM6	0.866	26.07	76.28	17.22	0.533	0.231	37
CH23	−5.74/−3.82	1.39	PM6	0.876	26.64	80.45	18.77	0.538	0.237	38
CH8F	−5.78/−3.80	—	D18	0.899	26.01	80.38	18.80	—	0.177	39
CH45	−5.66/−3.85	1.37	PM6	0.910	25.57	78.0	18.15	0.526	0.212	40
CH22	−5.67/−3.83	1.39	PM6	0.884	26.74	80.62	19.06	0.530	0.230	35
CH-F	−5.62/−3.86	1.33	PM6	0.875	26.21	75.59	17.34	0.525	0.212	41
CH-CF	−5.65/−3.85	1.37	PM6	0.886	26.07	76.30	17.62	0.534	0.240	41
CH-FCF	−5.67/−3.84	1.38	PM6	0.897	26.02	78.86	18.41	0.545	0.242	41
AQx-18	−5.63/−3.85	1.40	D18	0.938	25.0	77.8	18.2	0.537	0.200	42
AQx-2F	−5.62/−3.88	—	D18	0.937	26.1	80.4	19.7	0.518	0.194	36
CH17	−5.65/−3.86	1.36	PM6	0.883	26.19	77.2	17.84	0.50	0.19	43
TPQx-4F	−5.57/−3.74	1.41	PM6	0.94	14.96	54.41	7.72	—	—	44
TPQx-6F	−5.61/−3.78	1.43	PM6	0.92	21.83	70.94	14.30	—	—	44
QX-THF	−5.81/−4.08	1.40	PM6	0.902	24.49	78.99	17.45	—	—	45
Qx-H	−5.59/−3.92	1.41	PM6	0.922	20.78	73.77	14.11	0.521	0.205	46
Qx-Cl	−5.65/−3.95	1.44	PM6	0.913	24.13	78.32	17.25	0.533	0.217	46
Qx-Br	−5.64/−3.95	1.44	PM6	0.915	24.27	78.47	17.42	0.526	0.214	46
TPTC0	−5.64/−3.86	1.39	PM6	0.913	25.40	76.35	17.70	0.503	0.193	47
YB2T	−5.73/−3.89	1.38	PM6	0.918	24.48	75.85	17.05	0.556	0.236	48
CH-ThCl	−5.67/−3.78	—	PM6	0.934	25.43	76.45	18.16	0.519	0.211	49
CH-BBQ	−5.83/−3.88	1.35	PM6	0.881	26.15	78.9	18.19	0.567	0.242	50
Py1	−5.66/−4.04	1.33	PM1	0.736	25.29	63.3	11.78	—	—	51
Py2	−5.73/−3.98	1.33	PM1	0.871	26.83	75.9	17.73	—	—	51
Py3	−5.73/−4.00	1.34	PM1	0.869	25.65	72.5	16.15	—	—	51
Py4	−5.71/−4.02	1.35	PM1	0.817	18.04	50.9	7.40	—	—	51
Py5	−5.78/−3.95	1.35	PM1	0.890	23.32	76.5	15.87	—	—	51
Qo1	−5.69/−4.02	1.41	PM6	0.861	24.5	74.7	15.8	—	—	52
Qo2	−5.73/−4.01	1.41	PM6	0.894	26.6	77.3	18.4	—	—	52
Qo3	−5.75/−4.00	1.44	PM6	0.955	23.8	73.5	16.7	—	—	52
Qx-BO-1	−5.56/−3.74	1.46	PM6	0.956	18.21	60.64	10.57	0.503	0.189	53
Qx-BO-2	−5.50/−3.80	1.47	PM6	0.963	19.18	61.49	11.34	0.507	0.186	53
Qx-BO-3	−5.64/−3.84	1.41	PM6	0.889	24.76	77.39	17.03	0.550	0.229	53
AQx-6	−5.61/−3.86	1.32	D18	0.892	26.8	77.8	18.6	0.518	0.198	14
AQx-8	−5.60/−3.85	1.33	D18	0.913	24.7	75.7	17.1	0.493	0.178	14

been introduced into the Qx core, allowing numerous innovations in the realization of efficient acceptors with extended conjugated and precisely halogenated central units, ultimately boosting the photovoltaic performance of OSCs.

By replacing the central BT moiety in Y6 with more conjugated Qx derivatives, Wei and co-workers developed a pair of acceptors, named Qx-1 and Qx-2, to investigate the factors affecting the E_{loss} in devices.[34] Compared to Y6, these two acceptors show reduced reorganization energies due to the suppressed molecular vibration of the C–C bond stretching and thus decreased ΔE_2 and ΔE_3 (Fig. 3a–c). Moreover, the better aggregation patterns and longer exciton diffusion length of Qx-2 promote charge generation and transport in the corresponding device, thus a high PCE of 18.2% with a low ΔE_3 of 0.190 eV and an E_{loss} of 0.482 eV is achieved in the PM6:Qx-2-based OSCs. This work highlights the importance of the reorganization energy in achieving small energy loss and paves the way for obtaining high-performance OSCs. Since halogenation plays a crucial role in optimizing the properties of NFAs, they further developed a series of acceptors (Qx-*o*-4F, Qx-*m*-4F, Qx-*p*-4F, and Qx-*p*-4Cl) by performing precise central unit fluorination and end-group chlorination.[23] Different substitution positions of central fluorine atoms on these acceptors would significantly affect the local dipole moments and lead to distinct molecular packing behaviors, which are attributed to the interaction between the 1,1-dicyanomethylene-3-indanone (IC) terminal

© 2024 The Author(s). Published by the Royal Society of Chemistry

Open Access Article. Published on 07 maggio 2024. Downloaded on 18/04/2026 16:34:18.
This article is licensed under a Creative Commons Attribution-NonCommercial 3.0 Unported Licence.

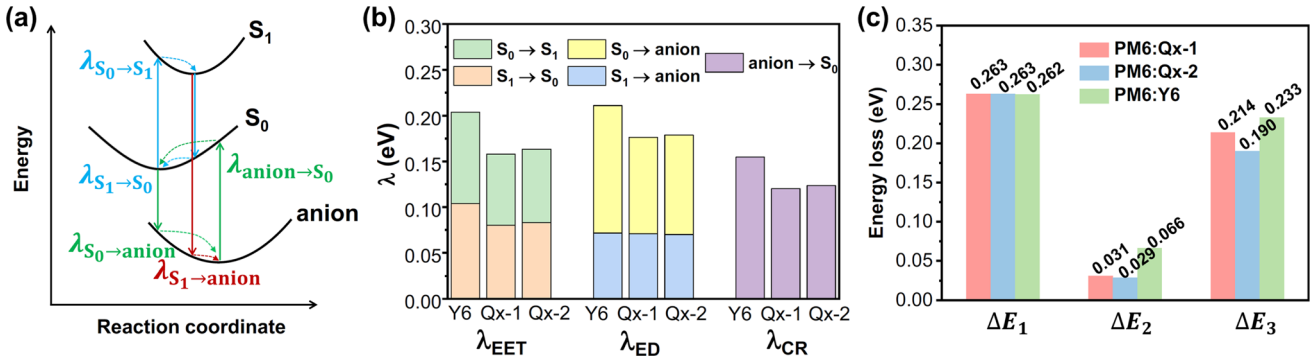

Fig. 3 (a) Illustration of the transitions among the ground state (S_0), the lowest singlet excited state (S_1), and the anionic state during the photoelectric conversion processes, taking the acceptor as an example. (b) The calculated reorganization energies for exciton diffusion (λ_{EET}, excitation energy transfer), exciton dissociation (λ_{ED}), and nonradiative charge recombination (λ_{CR}) at the tuned-ωB97XD/6-31G(d,p) level for Y6, Qx-1, and Qx-2. (c) Energy losses for OSCs based on different acceptors. Reproduced from ref. 32 with permission from the Nature Publishing Group, copyright [2022].

group and the fluorinated phenyl ring, the interaction between the IC terminal group and the thienothiophene (TT) unit, and the interaction between two IC terminal groups (Fig. 4d and e). Although Qx-*o*-4F exhibits more packing modes, it cannot form a well-connected charge transport network due to the large steric hindrance of the non-planar phenyl ring. In contrast, Qx-*m*-4F has good one-dimensional charge transport channels with strong π–π interaction. It is suggested that Qx-*p*-4F and Qx-*p*-4Cl can form a better charge transport network due to the enhanced local dipole moment, which is conducive to efficient charge transport. Furthermore, the end-group chlorination helps to broaden the absorption spectrum and decrease the energy loss, resulting in a PCE of 18.06% (18.78% after interlayer optimization) and a relatively low E_{loss} of 0.535 eV for PM6:Qx-*p*-4Cl-based OSCs. These results highlight the critical role of selective halogenation of central units and end groups in manipulating molecular packing, contributing to a better balance between V_{OC} and J_{SC} in OSCs.

Chen and co-workers have also extended the central Qx moiety to a phenazine moiety and developed a new acceptor CH4.[22] Although a small E_{loss} of 0.51 eV is achieved in the PM6:CH4-based device, a moderate PCE of 16.49% is delivered with an inferior FF of 71.1%. Inspired by the success of the end-group fluorination strategy in other Y-series acceptors, CH6 with a difluorophenazine central unit was developed. The fluorinated CH6 exhibits enhanced crystallinity and superior blend morphology, resulting in a significantly improved PCE of 18.33% with an E_{loss} of 0.53 eV for PM6:CH6-based OSCs. Based on the phenazine central unit, they developed a series of acceptors (CH-series) with different peripheral halogens in their subsequent studies to systematically investigate the effect of central unit halogenation of acceptors on their intermolecular packing behavior, film morphology, and the resulting photovoltaic performance in OSCs. For example, the regulation of fluorination and chlorination on both the central and end units gives rise to four acceptors, CH-6F, CH-4Cl, CH-6Cl, and CH23, with different molecular packing modes.[37,38] Among them, CH-4Cl, CH-6Cl, and CH23 exhibit several distinctive packing modes, including end unit to central unit ("E/C" mode), dual end unit to central unit ("dual E/C" mode), and dual end unit to bridge unit ("dual E/b" mode), which are not observed in the Y6 single crystal (Fig. 4a–c). Benefiting from their unique and superior packing modes, these acceptors, when blended with PM6, show favorable film morphologies, small energetic disorder, and more effective hybridization of CT and LE states, thus suppressing ΔE_3 in the relevant devices. In particular, CH23, with its increased packing density and dielectric properties, realizes a remarkable PCE of 18.77% along with a ΔE_3 of 0.237 eV and an E_{loss} of 0.538 eV in the resulting OSCs. Furthermore, they developed a new acceptor, CH8F, with a perfluorinated central unit.[39] Due to enhanced fluorine-induced secondary interactions and larger dipole moment, CH8F exhibits stronger and more ordered molecular packing compared to CH-6F, resulting in a larger dielectric constant and lower exciton binding energy. Consequently, OSCs based on D18:CH8F with favorable nanoscale morphology yield an excellent PCE of 18.80%. The iodization of the central unit has been used to enhance the intermolecular interaction and provides a novel acceptor, CH45.[40] Due to its increased molecular polarizability and reduced exciton binding energy, a PCE of 18.15% with a high V_{OC} of 0.910 V is realized in PM6:CH45-based OSCs. Considering that bromine has the additional advantages of greater crystallinity and easier polarization than fluorine and chlorine, they have recently developed a new acceptor, CH22, with a brominated central unit.[35] The bromination on the central unit contributes to enhancing the crystallinity and dielectric constant of the acceptor without compromising the favorable intermolecular packing created by end groups. Consequently, PM6:CH22-based binary OSCs afford an impressive PCE of 19.06% and an acceptable E_{loss} of 0.530 eV, along with decent thermal stability.

The asymmetric halogenation strategy has also been applied to the subtle modification of the Qx-based central unit. Lu and co-workers carried out direct fluorination and indirect trifluoromethylation on the central phenazine unit and constructed three acceptors, CH-F, CH-CF, and CH-FCF.[41] Among

Open Access Article. Published on 07 maggio 2024. Downloaded on 18/04/2026 16:34:18.
This article is licensed under a Creative Commons Attribution-NonCommercial 3.0 Unported Licence.

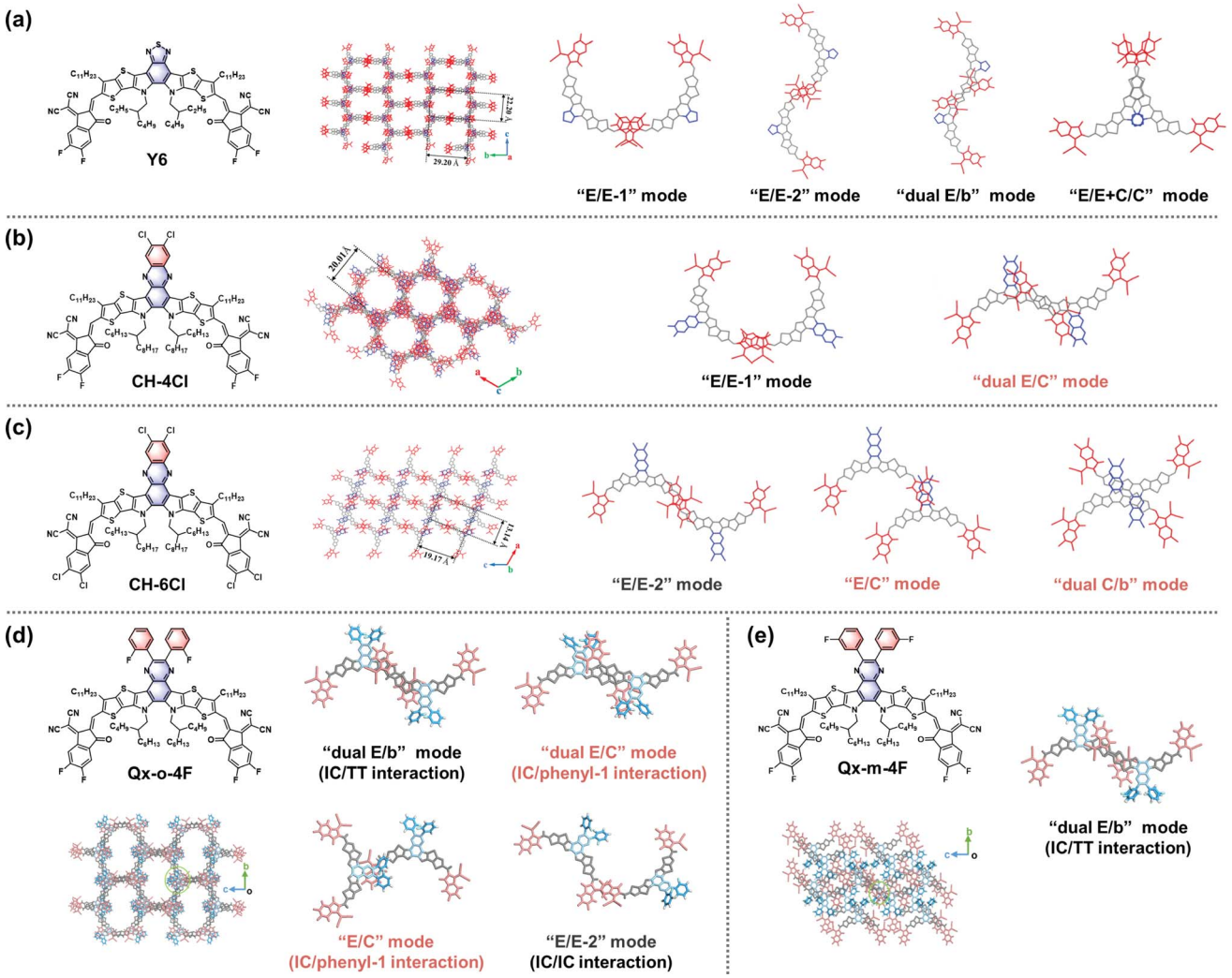

Fig. 4 Chemical structures, single crystal packing diagrams, and intermolecular packing modes of (a) Y6, (b) CH-4Cl, (c) CH-6Cl, (d) Qx-*m*-4F, and (e) Qx-*o*-4F. Reproduced from ref. 37 with permission from the Royal Society of Chemistry, copyright [2022]. Reproduced from ref. 23 with permission from the Royal Society of Chemistry, copyright [2023].

them, CH-FCF with both the fluorine and trifluoromethyl substitutions on the central unit shows enhanced intermolecular interactions and crystallinity, contributing to the formation of fibrillar network morphology with superior charge generation/transport. As a result, OSCs based on PM6:CH-FCF realize a high PCE of 18.41%. On the basis of L8BO, Zhu and co-workers synthesized a two-dimensional (2D) conjugated acceptor (AQx-18) with fluorine and chlorine atoms on the central unit, which exhibits ordered and compact molecular packing, resulting in a PCE of 18.2% when blended with D18.[42] In addition, they have recently developed an extended conjugated acceptor (AQx-2F) with a selectively fluorinated central unit.[36] Benefiting from an appropriate energy offset and a favorable fibril morphology with superior exciton/charge carrier dynamics, D18:AQx-2F-based binary OSCs achieve a fine balance between V_{OC} and J_{SC}, realizing a record PCE of 19.7% with a high V_{OC} of 0.937 V and a low E_{loss} of 0.518 eV, while exhibiting decent operational stability and retaining 83% of their initial PCE under maximum power point tracking for 500 hours.

The π-conjugated extension on both the central unit and end groups is another available method to manipulate the intermolecular stacking of acceptors. For example, Chen and co-workers reported a conjugation-extended acceptor, CH17, featuring a phenazine-based core and naphthalene-based terminal groups.[43] Compared to Y6, CH17 with bi-directional extended conjugation exhibits a more compact 3D molecular packing arrangement, leading to better charge transport, reduced energetic disorder, and suppressed ΔE_3. As a result, PM6:CH17-based OSCs yield a PCE of 17.84% along with a low E_{loss} of 0.50 eV and a ΔE_3 of 0.19 eV.

The introduction of halogenated thiophene into the Qx central core is a practical approach to tailoring the photoelectronic properties and aggregation behavior of acceptors. For example, Zou and co-workers developed two Qx-containing acceptors (TPQx-4F and TPQx-6F) with thiophene substituents

© 2024 The Author(s). Published by the Royal Society of Chemistry

Open Access Article. Published on 07 maggio 2024. Downloaded on 18/04/2026 16:34:18.
This article is licensed under a Creative Commons Attribution-NonCommercial 3.0 Unported Licence.

on the central unit.[44] Compared to TPQx-4F, TPQx-6F with fluorine atoms on the thiophene substituent shows more uniform nanophase aggregation when blended with PM6, resulting in a higher PCE of 14.30% in binary OSCs (7.72% for PM6:TPQx-4F-based OSCs). Similarly, based on efficient BTP-eC9, Ge and co-workers replaced the central unit with a fluorinated thiophene-substituted Qx core and synthesized QX-THF.[45] Due to enhanced intermolecular interaction and optimized film morphology, PM6:QX-THF-based OSCs yield a PCE of 17.45%. These results demonstrate that the fluorinated thiophene ring is a promising building block for Qx-based acceptors. In addition, Wei and co-workers have developed three acceptors (Qx-H, Qx-Cl, and Qx-Br) with different halogenated thiophene substitutions on the Qx core.[46] Compared to Qx-H without halogen atoms on the thiophene moiety, Qx-Br and Qx-Cl show enhanced absorption, improved crystallinity, and favorable film morphology, contributing to efficient charge transport. Consequently, a PCE of 17.42% with a V_{OC} of 0.915 V is realized in PM6:Qx-Br-based OSCs. Apart from the conjugated extension *via* a rotatable single bond, the thiophene ring was fused into the central Qx moiety to build large 2D conjugated acceptors. For example, Wei and co-workers reported an acceptor (TPTC0) with fused thiophene rings on the central unit.[47] The extended and rigid planar structure is conducive to molecular aggregation, resulting in high crystallinity and appropriate phase separation, giving a PCE of 17.70% with a low E_{loss} of 0.503 eV for PM6:TPTC0-based OSCs. The halogen atoms have also been introduced into the thiophene-fused Qx-containing central unit to optimize the molecular aggregation properties. For example, He and co-workers synthesized a 2D conjugated acceptor, YB2T, with fused bromothiophene rings on the central core.[48] The ordered and tight intermolecular stacking of YB2T enables the formation of a suitable phase separation structure when blended with a donor, contributing to efficient exciton dissociation and charge transport. Accordingly, a PCE of 17.05% is achieved in PM6:YB2T-based OSCs. Chen and co-workers also incorporated chlorothiophene rings into the phenazine-fused core and developed a new 2D conjugated acceptor, CH-ThCl.[49] The more extended conjugated central unit with chlorine substitution enhances the acceptor's PLQY and suppresses ΔE_3 in the resulting device. As a result, the PM6:CH-ThCl-based device achieves an excellent PCE of 18.16% with a high V_{OC} of 0.934 V, due to its relatively low ΔE_3 of 0.21 eV and E_{loss} of 0.519 eV.

In addition to the benzene and thiophane moieties, various heteroaromatic rings have been incorporated into the central Qx moiety, resulting in novel conjugation-extended central units that are advantageous for regulating the energy levels, intramolecular stacking, and crystallization behavior of acceptors. For example, Chen and co-workers developed a conjugation-extended acceptor (CH-BBQ) with a benzobisthiadiazole-fused Qx core that exhibits suitable energy levels, enhanced crystallinity, and desirable film morphology, resulting in a PCE of 18.19% for binary OSCs blended with PM6.[50] Moreover, Yang and co-workers reported a series of acceptors (Py-series, Py1–Py5) containing a pyridoquinoxaline core with chlorine substitution at different positions.[51] Compared to the non-chlorinated Py1, the chlorinated acceptors show enlarged optical band gaps. Among them, the *ortho*-chlorinated Py2 exhibits a larger dipole moment and tighter molecular stacking than other chlorinated isomers, contributing to favorable aggregation behaviors, resulting in a PCE of 17.73% for PM1:Py2-based OSCs. In addition, the introduction of intermolecular hydrogen-bonding interactions is a feasible strategy for tuning molecular packing patterns. Luo and co-workers incorporated methylated indanone moieties into the Qx core and synthesized three acceptors called Qo1, Qo2, and Qo3.[52] Among them, Qo2 shows multiple and stronger hydrogen-bonding interactions, contributing to a superior 3D charge transport network and achieving an excellent PCE of 18.4% for PM6:Qo2-based OSCs. Significantly, the optimal device exhibits satisfactory thermal stability, retaining 83% of its initial PCE after thermal aging at 65 °C for 250 hours.

To sum up, the strategy of π-conjugated extension combined with halogenation for Qx-based acceptors plays a crucial role in adjusting their intermolecular packing, optimizing the film morphology and suppressing energy loss. The binary OSCs based on acceptors with a precisely halogenated central unit have achieved a champion PCE of 19.7% with a low E_{loss} of 0.518 eV (ΔE_3 < 0.20 eV).[36] Therefore, subtle modification of the central unit has great potential to construct novel acceptors and further promote the development of efficient OSCs.

2.1.2 Side-chain modification of Qx-based SMAs. As mentioned above, Y-series acceptors have four independent side chains: two are attached to the β-positions of the outer thiophene units, and the other two are attached to the nitrogen atoms of the pyrrole rings. Side-chain modification of Y-series acceptors is an effective approach to tuning their solubility, absorption properties, molecular aggregation, and the corresponding device performance.

Inspired by the successful design of L8-BO, we have recently reported three Qx-based acceptors, Qx-BO-1, Qx-BO-2, and Qx-BO-3, containing 2-butyloctyl side chains at the β-positions of the outer thiophene units.[53] The introduction of branched alkyl chains enables high V_{OC} values of over 0.95 V with a low E_{loss} of around 0.50 eV for OSCs based on PM6:Qx-BO-1 and PM6:Qx-BO-2. However, their large central units and branched alkyl chains exhibit undesirable steric hindrance, resulting in inferior film morphology, which affects charge generation/transport and the resulting PCE (<12%). In contrast, Qx-BO-3 with a smaller Qx core shows suitable aggregation morphology and more efficient charge transport, resulting in a better balance among J_{SC}, V_{OC}, and FF and thus a higher PCE of about 17.0% in the PM6:Qx-BO-3-based device despite the largest E_{loss} (0.550 eV). This work demonstrates the importance of fine-tuning the size of the central unit in order to achieve rational side-chain modification.

In addition, Zhu and co-workers proposed that prolonged alkyl side chains contribute to a reduced free volume ratio (FVR), which restricts molecular motion in the solid state.[14] Specifically, they developed two acceptors, AQx-6 and AQx-8, with gradually extended alkyl chains at the nitrogen position of the pyrrole rings. The decreased FVRs for these two acceptors are beneficial for reducing electron-phonon coupling and

Open Access Article. Published on 07 maggio 2024. Downloaded on 18/04/2026 16:34:18.
This article is licensed under a Creative Commons Attribution-NonCommercial 3.0 Unported Licence.

suppressing ΔE_3 in the relevant devices. However, the side-chain length also affects the phase separation and crystallinity in blend films, thus influencing photophysical processes in OSCs. Significantly, AQ-6 with asymmetric side chains shows good miscibility with the donor D18, resulting in favorable film morphology with suitable separation and compact molecular packing, achieving a better balance between low ΔE_3 for high V_{OC} and efficient charge generation/transport for high J_{SC}. Consequently, D18:AQx-8-based OSCs deliver an impressive PCE of 18.6% with an E_{loss} of 0.518 eV and a small ΔE_3 of 0.198 eV.

2.2 Qx-based giant dimeric acceptors

The newly developed giant dimeric acceptors have attracted wide attention because of their unique advantages of a well-defined molecular structure, high efficiency, and excellent long-term stability.[54–56] Generally, giant dimeric acceptors are synthesized by linking the end groups of two Y-series SMAs *via* a π-spacer ("End group coupling"). In order to tune the molecular packing and improve the device performance, massive efforts have been devoted to π-spacer modification to improve the backbone planarity of giant dimeric acceptors.[20,57]

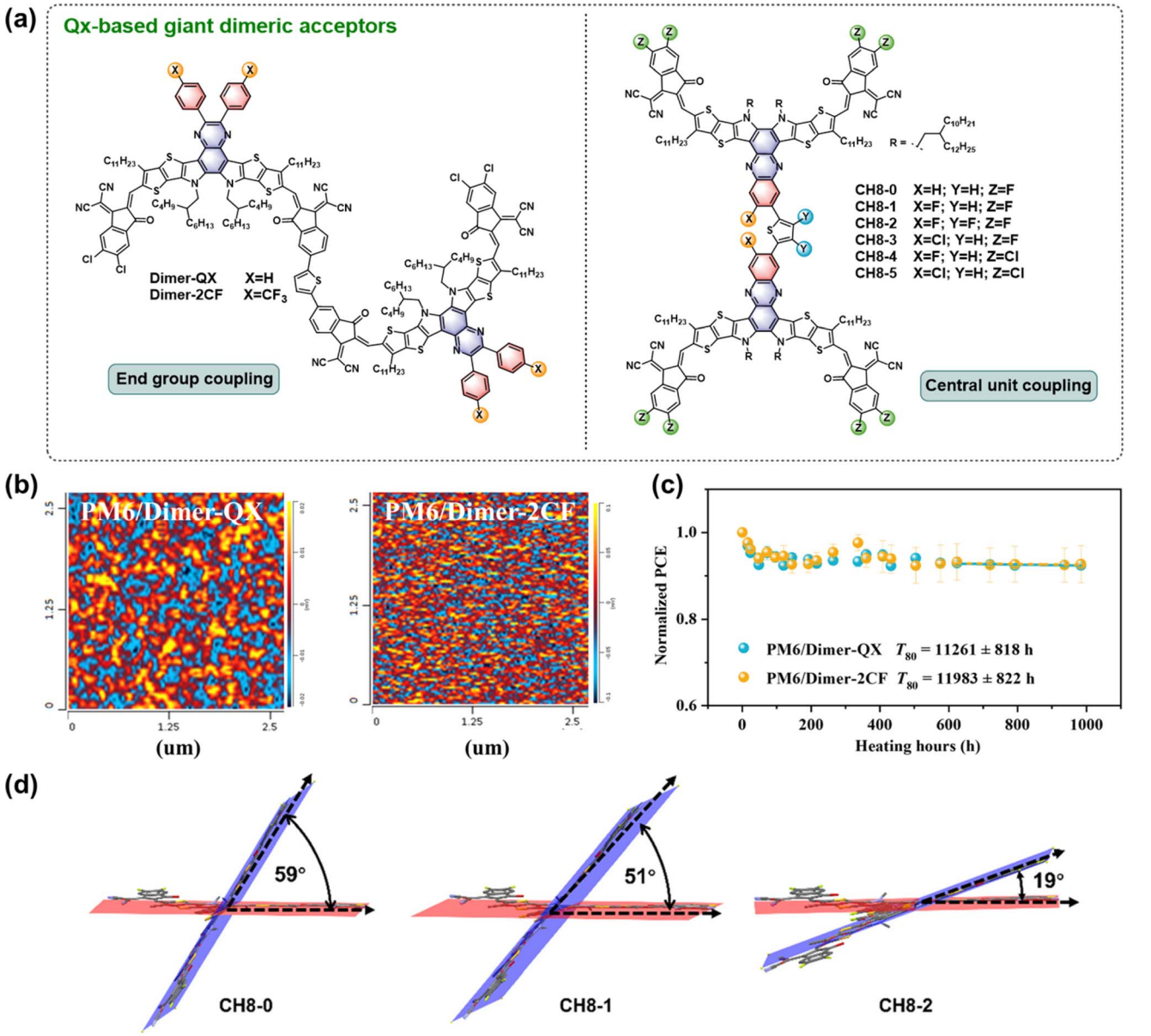

Fig. 5 (a) Chemical structures of Qx-based giant dimeric acceptors. (b) Atomic force microscopy-infrared spectroscopy (AFM-IR) images of PM6:Dimer-QX and PM6:Dimer-2CF blend films (measured at a characteristic wavenumber of these two dimeric acceptors, 1532 cm^{-1}). (c) Normalized PCEs of PM6:Dimer-QX and PM6:Dimer-2CF-based devices heating at 80 °C for 1000 hours. Reproduced from ref. 58 with permission from Wiley, copyright [2023]. (d) Ground-state geometries of CH8-0, CH8-1 and CH8-2 calculated by the DFT method, with the dihedral angles between two monomer planes marked. Reproduced from ref. 59 with permission from the Royal Society of Chemistry, copyright [2023].

© 2024 The Author(s). Published by the Royal Society of Chemistry

Open Access Article. Published on 07 maggio 2024. Downloaded on 18/04/2026 16:34:18.
This article is licensed under a Creative Commons Attribution-NonCommercial 3.0 Unported Licence.

In addition to the π-spacer, the resulting performance is largely related to the monomer. Therefore, Qx-based acceptors are promising candidates for giant units due to their multiple modification sites on the central unit, which are advantageous for optimizing the aggregation properties of acceptors and allow a novel coupling approach by linking the central units ("Central unit coupling").

Recently, Deng and co-workers reported two novel Qx-based giant dimeric acceptors, Dimer-QX and Dimer-2CF, without/with trifluoromethyl substitution on the central unit (Fig. 5a).[58] The introduction of trifluoromethyl with strong electronegativity reduces the surface energy of Dimer-2CF and enhances its electrostatic interaction with the donor PM6, contributing to favorable vertical phase distribution, suitable phase separation (Fig. 5b), and ordered molecular packing. The superior morphology endows Dimer-2CF-based OSCs with efficient exciton dissociation and charge transport, resulting in an excellent PCE of 18.12% (19.02% after interlayer optimization) with a high FF of 80.62% (Table 2). Significantly, both Dimer-QX and Dimer-2CF possess a high glass transition temperature (*ca.* 115 °C), which imparts excellent thermal stability to the resulting OSCs (Fig. 5c), retaining above 90% of their initial efficiencies after continuous heating at 80 °C for 1000 hours (extrapolated $T_{80} \approx 12\,000$ h). Moreover, both Dimer-based OSCs exhibit good photostability, with an extrapolated T_{80} lifetime of around 2500 h. This work highlights the importance of controlling hetero-molecular interactions and demonstrates the great potential of Qx-based giant dimeric acceptors for the construction of highly efficient and stable OSCs.

In order to release more end groups for efficient molecular packing, Chen and co-workers developed a series of giant dimeric acceptors (CH8-series) by linking the central units of two CH-series SMAs *via* a thiophene spacer. Selective fluorination was applied to the central phenazine moiety and the thiophene spacer, leading to gradually decreased dihedral angles between the two monomers from CH8-0 to CH8-1 to CH8-2 (Fig. 5d), caused by different strengths of noncovalently conformational locks *via* F–S/F–H secondary interactions between the central moiety and the spacer.[59] Benefiting from the low electron recombination energy, fibrillar network film morphology, and enhanced charge transport, OSCs based on PM6:CH8-1 achieve a PCE of 17.05%, along with decent thermal/photo-stability. Furthermore, selective chlorination was employed to the central unit and end groups of giant dimeric acceptors, giving CH8-3, CH8-4, and CH8-5.[60] From the fluorinated end groups to the chlorinated end groups, the resulting acceptors (CH8-4 and CH8-5) exhibit red-shifted absorption and enhanced crystallinity, affording a champion PCE of 17.58% for PM6:CH8-4-based OSCs. Importantly, devices based on CH8-3/4/5 show satisfactory thermal and photostability, retaining around 90% and 80% of their initial efficiencies after thermal aging at 65 °C for 430 h and continuous one-sun illumination for 250 h, respectively. The decent device stability could be partially attributed to the excellent morphological stability induced by both the strong intermolecular π–π stacking and the weak noncovalent interactions. These results demonstrate a novel and feasible strategy to construct promising multidimensional acceptors *via* central unit coupling towards efficient and stable OSCs.

2.3 Qx-based polymeric acceptors

All-polymer solar cells (all-PSCs) have also drawn tremendous attention due to their superior morphological stability and great mechanical flexibility.[61,62] However, limited by the lack of efficient polymeric acceptors, the efficiencies of all-PSCs still lag behind those of SMA-based OSCs. Impressively, polymerized small molecule acceptors (PSMAs) have achieved great success by inheriting the excellent properties of SMAs.[63] To further improve the performance of all-PSCs, various structural modification strategies involving the SMA monomer and the linking unit have been developed. In particular, Qx-based polymeric

Table 2 The photovoltaic parameters of Qx-based giant dimeric and polymeric acceptors

Acceptor	HOMO/LUMO [eV]	*E*gopt [eV]	Donor	V_{OC} [V]	J_{SC} [mA cm^{-2}]	FF [%]	PCE [%]	E_{loss} [eV]	ΔE_3 [eV]	Ref.
Dimer-QX	−5.52/−3.77	1.40	PM6	0.933	22.57	69.26	14.59	—	—	58
Dimer-2CF	−5.57/−3.78	1.41	PM6	0.889	25.27	80.62	18.12	—	—	58
CH8-0	−5.61/−3.78	1.41	PM6	0.936	22.61	72.1	15.26	0.490	0.182	59
CH8-1	−5.69/−3.80	1.42	PM6	0.923	24.89	74.2	17.05	0.518	0.206	59
CH8-2	−5.71/−3.81	1.44	PM6	0.928	24.24	74.9	16.84	0.529	0.213	59
CH8-3	−5.74/−3.76	1.44	PM6	0.915	24.44	77.0	17.22	0.529	0.214	60
CH8-4	−5.75/−3.79	1.40	PM6	0.894	26.05	75.5	17.58	0.518	0.193	60
CH8-5	−5.76/−3.79	1.41	PM6	0.902	24.75	75.2	16.79	0.520	0.206	60
PQx1	−5.56/−3.75	1.43	PM6	0.951	17.36	59.05	9.75	0.494	0.173	64
PQx2	−5.55/−3.72	1.44	PM6	0.899	5.63	51.61	2.61	0.535	0.208	64
PQx3	−5.60/−3.76	1.45	PM6	0.932	24.79	76.17	17.60	0.518	0.191	64
PZC16	−5.61/−3.81	1.43	PM6	0.861	18.98	56.65	9.22	0.599	0.291	65
PZC17	−5.60/−3.79	1.44	PM6	0.926	23.35	75.54	16.33	0.534	0.236	65
PZC1	−5.69/−3.72	1.44	PM6	0.923	22.10	67.88	13.83	—	—	66
PZC2	−5.62/−3.74	1.45	PM6	0.936	24.61	74.93	17.30	—	—	66
PZC3	−5.64/−3.75	1.46	PM6	0.953	22.34	73.97	15.75	—	—	66
SH-1	−5.68/−3.69	1.45	PM6	0.979	21.03	68.67	14.14	0.522	0.203	67
SH-2	−5.64/−3.76	1.38	PM6	0.908	12.87	55.94	6.55	0.529	0.224	67

Open Access Article. Published on 07 maggio 2024. Downloaded on 18/04/2026 16:34:18.
This article is licensed under a Creative Commons Attribution-NonCommercial 3.0 Unported Licence.

acceptors have great potential to construct highly efficient all-PSCs by virtue of their unique molecular packing properties and abundant modification sites.

In terms of the SMA monomer, its molecular structure, particularly the central unit substitutions, has a significant effect on the molecular interactions and aggregation behavior during the blend film formation process. Lu and co-workers have recently reported three Qx-based PSMAs, PQx1, PQx2, and PQx3 (Fig. 6a), featuring different central unit substitutions.[64] As shown in Fig. 6b–d, the difference in the central unit affects the crystallinity of these polymeric acceptors and their miscibility with PM6. Among them, PQx-3 shows appropriate aggregation ability and intermolecular interaction, resulting in optimal blend morphology with suitable phase separation and superior charge transport properties. In contrast, PQx1 and PQx2 exhibit insufficient or excessive crystallinity, giving unsatisfactory blend morphologies. Consequently, PQx-3-based binary all-PSCs achieve an excellent PCE of 17.60% (9.75% and 2.61% for PQx1- and PQx-2-based devices, respectively), which is further improved to 18.82% in ternary all-PSCs. In addition, due to their superior morphological stability, PM6:PQx-3-based devices exhibit better thermal stability with a T_{80} lifetime of about 160 h compared to PQx-1/PQx-2-based devices ($T_{80} \approx 50$ h).

In terms of the linking unit, Chen and co-workers have developed a range of Qx-based polymeric acceptors (PZC-series) to investigate the effect of linking unit modification on the optoelectronic and molecular aggregation properties of polymeric acceptors. To reduce the molecular torsion caused by the traditional aromatic linkers, they synthesized two PSMAs with non-aromatic linkers (ethynyl for PZC16 and vinylene for PZC17). Both polymeric acceptors show good planarity of the conjugated backbones and similar energy levels, while PZC17 shows better miscibility with the donor PM6, leading to a suitable phase separation in blend films. Therefore, PZC17-based all-PSCs deliver a higher PCE (16.33%) than PZC16-based devices (9.22%).[65] In addition, three polymeric acceptors (PZC1, PZC2, and PZC3) were developed by introducing halogen atoms on the thiophene linker.[66] Among them, PZC2 with a fluorinated thiophene linker exhibits a more planar molecular conformation and optimal morphology in blend films, contributing to efficient charge dynamics. As a result, PZC2-based all-PSCs achieve an excellent PCE of 17.30% (13.83% and 15.75% for PZC1- and PZC3-based devices, respectively),

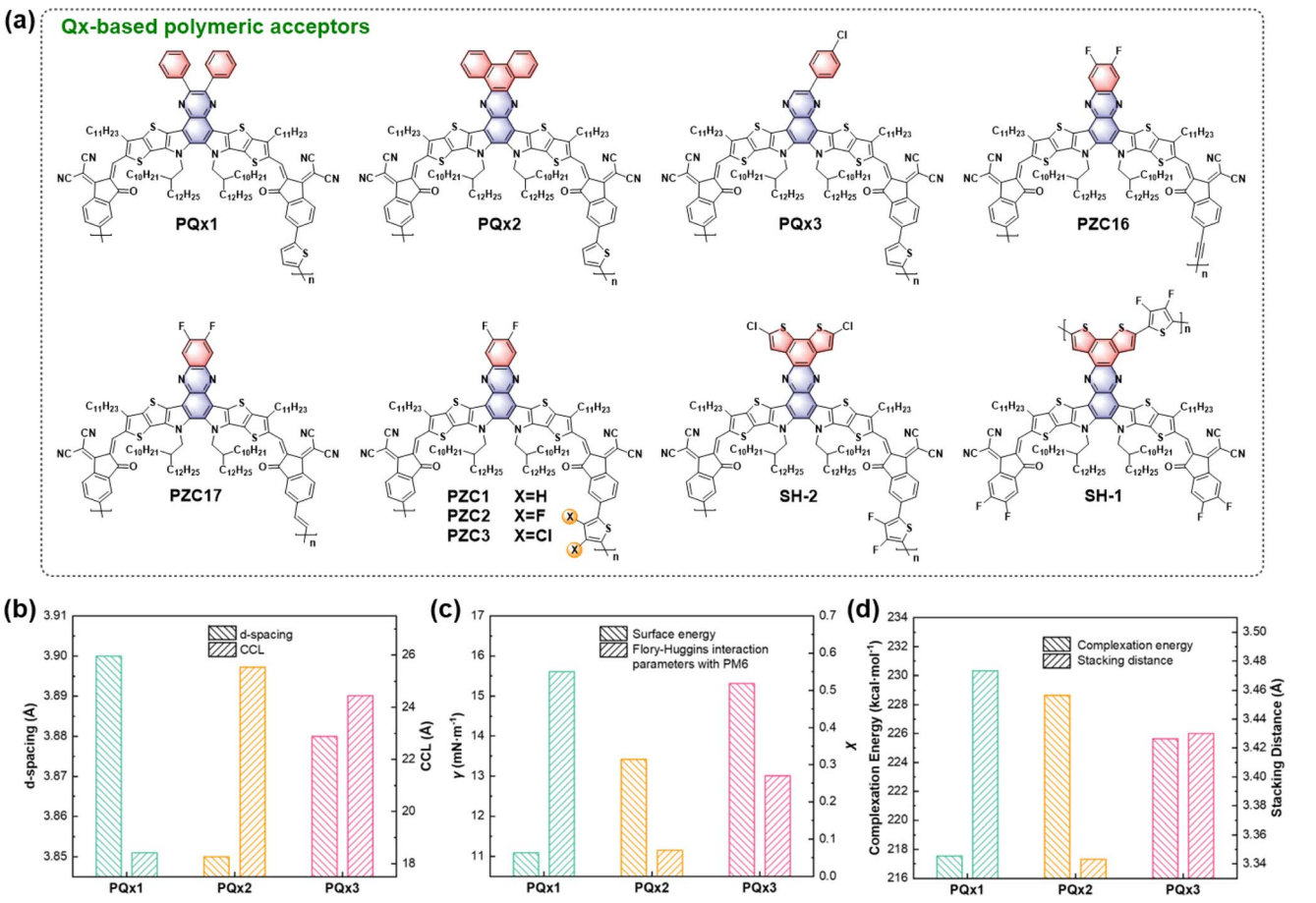

Fig. 6 (a) Chemical structures of Qx-based polymeric acceptors. (b) π–π stacking *d*-spacing and crystalline coherent length (CCL) of PQx1, PQx2, and PQx3 neat films. (c) Surface energy of the three polymeric acceptors and the Flory–Huggins interaction parameters with PM6. (d) Complexation energy and stacking distances of three polymeric acceptors with PM6 according to the theoretical calculation. Reproduced from ref. 64 with permission from Wiley, copyright [2023].

© 2024 The Author(s). Published by the Royal Society of Chemistry

Open Access Article. Published on 07 maggio 2024. Downloaded on 18/04/2026 16:34:18.
This article is licensed under a Creative Commons Attribution-NonCommercial 3.0 Unported Licence.

while exhibiting the best thermal stability, partly due to the stable morphology induced by the coplanar molecular conformation.

In addition to the polymerization between the end groups of two SMAs, the polymerization between the central units has been developed to produce novel Qx-based polymeric acceptors. Based on CH-series SMAs, Chen and co-workers reported a polymeric acceptor, SH-1, by central unit polymerization.[67] Compared to the end-group polymerized SH-2, SH-1 exhibits more ordered intermolecular packing and favorable morphology in blend films, contributing to efficient exciton dissociation and charge transport. Therefore, PM6:SH-1-based devices deliver significantly higher PCE (14.14%) than PM6:SH-2-based devices (6.55%). This work provides an alternative pathway to construct efficient polymer acceptors through the delicate design of both the central building block and the linking unit.

2.4 Ternary strategy by introducing Qx-based acceptors

The ternary strategy, namely incorporating an additional donor or acceptor into the binary system, is an effective way to improve the photovoltaic performance of OSCs. The introduction of a suitable third component commonly contributes to complementary absorption coverage, morphology optimization, and energy loss mitigation, resulting in an outstanding PCE of over 19.5% in the state-of-the-art ternary organic solar cells (TOSCs).[5,6] As previously discussed, Qx-based NFAs exhibit structural diversity, superior molecular aggregation properties, and reduced energy loss, enabling them to be a third component to construct efficient TOSCs with decreased E_{loss}.

To fine-tune the optoelectronic properties and morphology of the typical PM6:Y6 binary system, Zhu and coworkers conceived a "two-in-one" strategy by incorporating a Qx-containing acceptor, AQx-3 (Fig. 7a).[68] These two acceptors (AQx-3 and Y6), with high structural similarity and compatibility, form an alloy-like composite that is conducive to adjusting the HOMO offset and optimizing the film morphology, thereby enhancing charge generation/transport and reducing E_{loss}. Thus, the optimal TOSCs (PM6 : Y6 : AQx-3 = 1 : 0.8 : 0.4) realize an impressive PCE of over 18% (Table 3), which is the highest value reported at that time for Y6-based TOSCs.

Encouraged by the PM6:Qx2 system with low energy loss, Wei and co-workers further constructed efficient TOSCs based on PM6:*m*-BTP-PhC6:Qx2 with simultaneously increased V_{OC}, J_{SC}, and FF.[69] The third component Qx2 promotes the miscibility between the donor and the acceptor composite in the resulting ternary blend, leading to ideal film morphology and thus decreased energetic disorder, improved charge extraction, and reduced E_{loss} (Fig. 7b and c) in the optimum TOSCs. As a result, PM6:*m*-BTP-PhC6:Qx2-based TOSCs deliver a champion PCE of 17.97% (18.62% after interlayer optimization) with

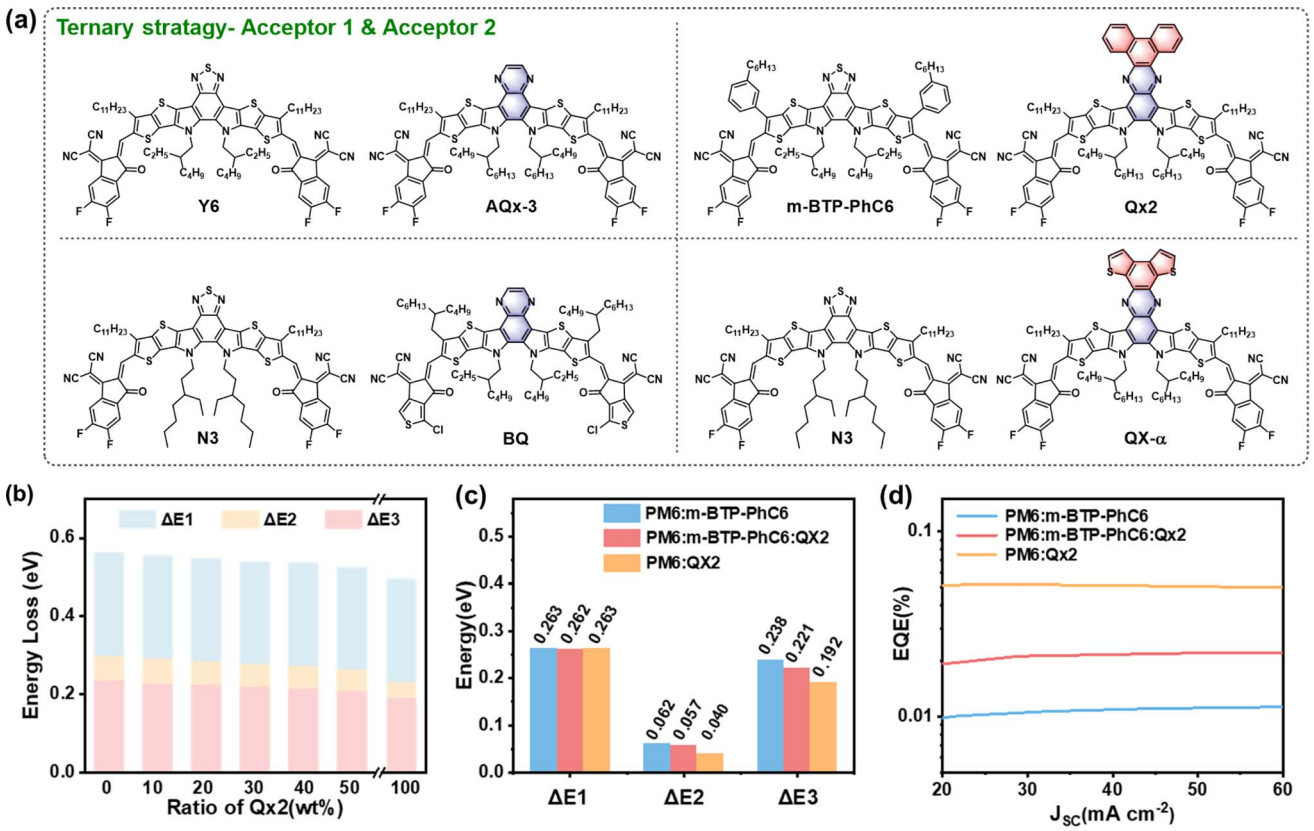

Fig. 7 (a) Chemical structures of acceptors of ternary systems discussed in this perspective. (b) Variation tendency in the energy losses of devices with different Qx2 ratios. (c) Statistical diagram of detailed energy loss terms for the binary and optimal ternary devices. (d) EQE_{EL} curves of the binary and optimal ternary devices. Reproduced from ref. 69 with permission from the Royal Society of Chemistry, copyright [2023].

Open Access Article. Published on 07 maggio 2024. Downloaded on 18/04/2026 16:34:18.
This article is licensed under a Creative Commons Attribution-NonCommercial 3.0 Unported Licence.

Table 3 The photovoltaic parameters of TOSCs with Qx-based acceptors

Acceptor	HOMO/LUMO [eV]	Donor	V_{OC} [V]	J_{SC} [mA cm^{-2}]	FF [%]	PCE [%]	E_{loss} [eV]	Ref.
AQx-3	−5.64/−3.86	PM6	0.891	24.16	77.4	16.67	0.539	68
Y6	−5.70/−3.90	PM6	0.856	25.73	76.8	16.94	0.554	68
Y6:AQx-3	−5.69/−3.88	PM6	0.870	26.82	77.2	18.01	0.550	68
Qx2	−5.54/−3.86	PM6	0.935	24.28	75.37	17.11	0.493	69
m-BTP-PhC6	−5.59/−3.86	PM6	0.850	25.69	78.43	17.12	0.560	69
m-BTP-PhC6:Qx2	—	PM6	0.875	25.91	79.12	17.97	0.539	69
BQ	−5.56/−4.17	D18	0.959	21.27	69.35	14.14	—	70
N3	−5.70/−4.41	D18	0.827	27.53	78.04	17.77	0.562	70
N3:BQ	—	D18	0.846	27.92	79.95	18.89	0.547	70
QX-α	−5.64/−3.88	D18	0.944	24.67	69.9	14.30	—	71
N3	−5.79/−3.94	D18	0.832	27.98	78.0	18.16	0.587	71
N3:QX-α	—	D18	0.862	27.86	80.5	19.33	0.553	71

a significantly improved V_{OC} of 0.875 V (0.850 V for the PM6:*m*-BTP-PhC6 binary system).

Designing an appropriate third component based on the Qx core is a feasible approach to further improve the performance of existing efficient binary systems. Ge and co-workers synthesized a novel acceptor, BQ, featuring a Qx central unit and chlorinated thiophene end groups.[70] On the basis of the Qx core, the introduction of chlorinated thiophene on the end groups of the NFAs helps to regulate energy levels and suppress E_{loss}, leading to much-upshifted energy levels of BQ and thus a high V_{OC} of 0.959 V when blended with D18. After the addition of BQ to the D18:N3 binary system, cascade-like model TOSCs are realized with undisturbed nanofiber network morphology, enhanced charge transfer/collection, and reduced energy loss. Eventually, the resulting TOSCs achieve an increased PCE of 18.89% with a decreased E_{loss} of 0.547 eV compared to the D18:N3-based binary OSCs (17.77% and 0.562 eV, respectively). In addition, they developed two isomeric acceptors (QX-α and QX-γ) with different orientations of fused thiophene rings on the Qx core.[71] Compared to QX-γ, QX-α has S–N noncovalent interactions, giving a larger dipole moment, more ordered molecular stacking, and a higher surface energy. By incorporating QX-α into D18:N3, the resulting TOSCs show more balanced charge mobilities, enhanced charge collection, and suppressed energy loss than D18:N3-based binary OSCs, yielding a champion PCE of 19.33% with obviously increased V_{OC} and FF. These results demonstrate that Qx-based acceptors with delicate modification could serve as a suitable third component for the construction of highly efficient TOSCs.

3. Conclusions and outlooks

This perspective summarizes the design strategies and advances of Qx-based acceptors, including small-molecule, giant dimeric, and polymeric acceptors. Extensive efforts have offered a better understanding of the structure–property relationship of Qx-based acceptors, contributing to the realization of high-performance OSCs with lower energy loss and more efficient charge generation/transport. Due to the huge space for structural modification, Qx-based acceptors have great potential to achieve efficient and stable OSCs for commercial applications. Therefore, several directions for further studies in molecular design and device optimization for Qx systems are proposed.

(1) From a molecular design perspective, subtle structural modification can lead to significant improvements in device performance. Firstly, the incorporation of intermolecular noncovalent interactions *via* precise substituent engineering is a promising approach to regulating the molecular packing behavior of acceptors, which is conducive to further improving the charge transport properties. Secondly, other commercialized simple polycyclic aromatic/heteroaromatic moieties can be introduced into the central core to increase the photoluminescence quantum yield, which has great potential to reduce nonradiative energy loss. Synthetic complexity and scalability should also be considered. Additional side-chain or substituent engineering may be required to ensure sufficient solubility when extending the conjugated central core. Therefore, it is critical to control the size of the central unit and employ proper heteroatom replacement rather than over-extending the rigid conjugated plane. Thirdly, bilateral substitution of aromatic or heteroaromatic rings on the Qx core can be changed to unilateral substitution to improve reaction yields and fine-tune energy levels and molecular stacking, which is expected to achieve lower energy losses and further performance improvements. Fourthly, developing novel Qx-based dimeric and trimeric acceptors with a higher glass transition temperature could simultaneously improve the charge transport and long-term stability of the devices, thus realizing highly efficient and stable OSCs.

(2) From a device optimization perspective, the matching of donor/acceptor materials and the construction of ternary devices are essential approaches to accessing the lower limit of energy losses for a given material without sacrificing charge generation. Firstly, in addition to the commonly used PM6 donor, it is necessary to introduce other efficient donors with matched energy levels and suitable miscibility with Qx-based acceptors to form the desired nanoscale phase separation and ordered molecular packing in blend films. Secondly, the planar and rigid skeleton is likely to result in reduced reorganization energies and thus decreased energy loss, making Qx-based acceptors a promising third component for the construction

© 2024 The Author(s). Published by the Royal Society of Chemistry

Open Access Article. Published on 07 maggio 2024. Downloaded on 18/04/2026 16:34:18.
This article is licensed under a Creative Commons Attribution-NonCommercial 3.0 Unported Licence.

of highly efficient TOSCs. For existing Qx-based acceptors, efficient binary systems with appropriate interactions and miscibility should be sought to realize morphology control and energy loss reduction. Thirdly, the low energy loss Qx system provides an excellent platform for large-area roll-to-roll fabrication.[72] However, most Qx-based acceptors with a large rigid conjugated central unit have a strong molecular aggregation ability, which would induce excessive crystallinity and unfavorable phase separation during the film formation process. It is therefore necessary to manipulate the film formation kinetics of Qx systems in green solvents, further expanding the application prospects of materials with high crystallinity.

Author contributions

M. X. and K. L. conceived the idea. M. X. prepared the manuscript. Z. W. and K. L. directed and supervised the project. All authors discussed and commented on the manuscript.

Conflicts of interest

There are no conflicts to declare.

Acknowledgements

The authors acknowledge the financial support provided by the Beijing Natural Science Foundation (Grant No. Z230018) and the Strategic Priority Research Program of the Chinese Academy of Sciences (No. XDB36010200 and XDB0520102).

References

1 D. Wang, Y. Li, G. Zhou, E. Gu, R. Xia, B. Yan, J. Yao, H. Zhu, X. Lu, H.-L. Yip, H. Chen and C.-Z. Li, *Energy Environ. Sci.*, 2022, **15**, 2629–2637.
2 Z. Wang, Y. Bo, P. Bai, S. Zhang, G. Li, X. Wan, Y. Liu, R. Ma and Y. Chen, *Science*, 2023, **382**, 1291–1296.
3 J. Wang, Y. Wang, J. Li, Y. Yu, P. Bi, J. Qiao, Z. Chen, C. Wang, W. Wang, J. Dai, X. Hao, S. Zhang and J. Hou, *Angew. Chem., Int. Ed.*, 2023, **62**, e202314362.
4 T. Chen, S. Li, Y. Li, Z. Chen, H. Wu, Y. Lin, Y. Gao, M. Wang, G. Ding, J. Min, Z. Ma, H. Zhu, L. Zuo and H. Chen, *Adv. Mater.*, 2023, **35**, 2300400.
5 L. Zhu, M. Zhang, J. Xu, C. Li, J. Yan, G. Zhou, W. Zhong, T. Hao, J. Song, X. Xue, Z. Zhou, R. Zeng, H. Zhu, C. C. Chen, R. C. I. MacKenzie, Y. Zou, J. Nelson, Y. Zhang, Y. Sun and F. Liu, *Nat. Mater.*, 2022, **21**, 656–663.
6 P. Bi, J. Wang, Y. Cui, J. Zhang, T. Zhang, Z. Chen, J. Qiao, J. Dai, S. Zhang, X. Hao, Z. Wei and J. Hou, *Adv. Mater.*, 2023, **35**, 2210865.
7 B. Pang, C. Liao, X. Xu, L. Yu, R. Li and Q. Peng, *Adv. Mater.*, 2023, **35**, 2300631.
8 X.-K. Chen, D. Qian, Y. Wang, T. Kirchartz, W. Tress, H. Yao, J. Yuan, M. Hülsbeck, M. Zhang, Y. Zou, Y. Sun, Y. Li, J. Hou, O. Inganäs, V. Coropceanu, J.-L. Bredas and F. Gao, *Nat. Energy*, 2021, **6**, 799–806.
9 J. Jeong, M. Kim, J. Seo, H. Lu, P. Ahlawat, A. Mishra, Y. Yang, M. A. Hope, F. T. Eickemeyer, M. Kim, Y. J. Yoon, I. W. Choi, B. P. Darwich, S. J. Choi, Y. Jo, J. H. Lee, B. Walker, S. M. Zakeeruddin, L. Emsley, U. Rothlisberger, A. Hagfeldt, D. S. Kim, M. Gratzel and J. Y. Kim, *Nature*, 2021, **592**, 381–385.
10 J. Yuan, H. Zhang, R. Zhang, Y. Wang, J. Hou, M. Leclerc, X. Zhan, F. Huang, F. Gao, Y. Zou and Y. Li, *Chem*, 2020, **6**, 2147–2161.
11 J. Yao, T. Kirchartz, M. S. Vezie, M. A. Faist, W. Gong, Z. He, H. Wu, J. Troughton, T. Watson, D. Bryant and J. Nelson, *Phys. Rev. Appl.*, 2015, **4**, 014020.
12 M. Azzouzi, J. Yan, T. Kirchartz, K. Liu, J. Wang, H. Wu and J. Nelson, *Phys. Rev. X*, 2018, **8**, 031055.
13 S. Liu, J. Yuan, W. Deng, M. Luo, Y. Xie, Q. Liang, Y. Zou, Z. He, H. Wu and Y. Cao, *Nat. Photonics*, 2020, **14**, 300–305.
14 Y. Jiang, Y. Li, F. Liu, W. Wang, W. Su, W. Liu, S. Liu, W. Zhang, J. Hou, S. Xu, Y. Yi and X. Zhu, *Nat. Commun.*, 2023, **14**, 5079.
15 D. Qian, Z. Zheng, H. Yao, W. Tress, T. R. Hopper, S. Chen, S. Li, J. Liu, S. Chen, J. Zhang, X. K. Liu, B. Gao, L. Ouyang, Y. Jin, G. Pozina, I. A. Buyanova, W. M. Chen, O. Inganas, V. Coropceanu, J. L. Bredas, H. Yan, J. Hou, F. Zhang, A. A. Bakulin and F. Gao, *Nat. Mater.*, 2018, **17**, 703–709.
16 S. M. Hosseini, S. Wilken, B. Sun, F. Huang, S. Y. Jeong, H. Y. Woo, V. Coropceanu and S. Shoaee, *Adv. Energy Mater.*, 2023, **13**, 2203576.
17 F. D. Eisner, M. Azzouzi, Z. Fei, X. Hou, T. D. Anthopoulos, T. J. S. Dennis, M. Heeney and J. Nelson, *J. Am. Chem. Soc.*, 2019, **141**, 6362–6374.
18 Y. Xu, H. Yao, L. Ma, L. Hong, J. Li, Q. Liao, Y. Zu, J. Wang, M. Gao, L. Ye and J. Hou, *Angew. Chem., Int. Ed.*, 2020, **59**, 9004–9010.
19 Z. Zhang, Y. Li, G. Cai, Y. Zhang, X. Lu and Y. Lin, *J. Am. Chem. Soc.*, 2020, **142**, 18741–18745.
20 X. Gu, Y. Wei, N. Yu, J. Qiao, Z. Han, Q. Lin, X. Han, J. Gao, C. Li, J. Zhang, X. Hao, Z. Wei, Z. Tang, Y. Cai, X. Zhang and H. Huang, *CCS Chem.*, 2023, **5**, 2576–2588.
21 C. Yang, Q. An, M. Jiang, X. Ma, A. Mahmood, H. Zhang, X. Zhao, H. F. Zhi, M. H. Jee, H. Y. Woo, X. Liao, D. Deng, Z. Wei and J. L. Wang, *Angew. Chem., Int. Ed.*, 2023, **62**, e202313016.
22 H. Chen, H. Liang, Z. Guo, Y. Zhu, Z. Zhang, Z. Li, X. Cao, H. Wang, W. Feng, Y. Zou, L. Meng, X. Xu, B. Kan, C. Li, Z. Yao, X. Wan, Z. Ma and Y. Chen, *Angew. Chem., Int. Ed.*, 2022, **61**, e202209580.
23 M. Xie, Y. Shi, L. Zhu, J. Zhang, Q. Cheng, H. Zhang, Y. Yan, M. Zhu, H. Zhou, K. Lu and Z. Wei, *Energy Environ. Sci.*, 2023, **16**, 3543–3551.
24 Y. Lin, J. Wang, Z. G. Zhang, H. Bai, Y. Li, D. Zhu and X. Zhan, *Adv. Mater.*, 2015, **27**, 1170–1174.
25 Y. Lin, Q. He, F. Zhao, L. Huo, J. Mai, X. Lu, C. J. Su, T. Li, J. Wang, J. Zhu, Y. Sun, C. Wang and X. Zhan, *J. Am. Chem. Soc.*, 2016, **138**, 2973–2976.
26 J. Yuan, Y. Zhang, L. Zhou, G. Zhang, H.-L. Yip, T.-K. Lau, X. Lu, C. Zhu, H. Peng, P. A. Johnson, M. Leclerc, Y. Cao, J. Ulanski, Y. Li and Y. Zou, *Joule*, 2019, **3**, 1140–1151.

Open Access Article. Published on 07 maggio 2024. Downloaded on 18/04/2026 16:34:18.
This article is licensed under a Creative Commons Attribution-NonCommercial 3.0 Unported Licence.

27 Y. Cui, H. Yao, J. Zhang, K. Xian, T. Zhang, L. Hong, Y. Wang, Y. Xu, K. Ma, C. An, C. He, Z. Wei, F. Gao and J. Hou, *Adv. Mater.*, 2020, **32**, 1908205.
28 C. Li, J. Zhou, J. Song, J. Xu, H. Zhang, X. Zhang, J. Guo, L. Zhu, D. Wei, G. Han, J. Min, Y. Zhang, Z. Xie, Y. Yi, H. Yan, F. Gao, F. Liu and Y. Sun, *Nat. Energy*, 2021, **6**, 605–613.
29 D. Luo, Z. Jiang, C. Shan, L. Li, C. Duan, Q. Liu, Z. Wang, K. Wang, B. Xu and A. K. K. Kyaw, *ACS Appl. Mater. Interfaces*, 2022, **14**, 24374–24385.
30 D. Luo, W. Jang, D. D. Babu, M. S. Kim, D. H. Wang and A. K. K. Kyaw, *J. Mater. Chem. A*, 2022, **10**, 3255–3295.
31 G. Zhang, X. K. Chen, J. Xiao, P. C. Y. Chow, M. Ren, G. Kupgan, X. Jiao, C. C. S. Chan, X. Du, R. Xia, Z. Chen, J. Yuan, Y. Zhang, S. Zhang, Y. Liu, Y. Zou, H. Yan, K. S. Wong, V. Coropceanu, N. Li, C. J. Brabec, J. L. Bredas, H. L. Yip and Y. Cao, *Nat. Commun.*, 2020, **11**, 3943.
32 F. Lin, K. Jiang, W. Kaminsky, Z. Zhu and A. K. Jen, *J. Am. Chem. Soc.*, 2020, **142**, 15246–15251.
33 Z. Zhou, W. Liu, G. Zhou, M. Zhang, D. Qian, J. Zhang, S. Chen, S. Xu, C. Yang, F. Gao, H. Zhu, F. Liu and X. Zhu, *Adv. Mater.*, 2020, **32**, 1906324.
34 Y. Shi, Y. Chang, K. Lu, Z. Chen, J. Zhang, Y. Yan, D. Qiu, Y. Liu, M. A. Adil, W. Ma, X. Hao, L. Zhu and Z. Wei, *Nat. Commun.*, 2022, **13**, 3256.
35 H. Liang, X. Bi, H. Chen, T. He, Y. Lin, Y. Zhang, K. Ma, W. Feng, Z. Ma, G. Long, C. Li, B. Kan, H. Zhang, O. A. Rakitin, X. Wan, Z. Yao and Y. Chen, *Nat. Commun.*, 2023, **14**, 4707.
36 K. Liu, Y. Jiang, G. Ran, F. Liu, W. Zhang and X. Zhu, *Joule*, 2024, **8**, 835–851.
37 Y. Zou, H. Chen, X. Bi, X. Xu, H. Wang, M. Lin, Z. Ma, M. Zhang, C. Li, X. Wan, G. Long, Y. Zhaoyang and Y. Chen, *Energy Environ. Sci.*, 2022, **15**, 3519–3533.
38 H. Liang, H. Chen, P. Wang, Y. Zhu, Y. Zhang, W. Feng, K. Ma, Y. Lin, Z. Ma, G. Long, C. Li, B. Kan, Z. Yao, H. Zhang, X. Wan and Y. Chen, *Adv. Funct. Mater.*, 2023, **33**, 2301573.
39 Z. Yao, X. Cao, X. Bi, T. He, Y. Li, X. Jia, H. Liang, Y. Guo, G. Long, B. Kan, C. Li, X. Wan and Y. Chen, *Angew. Chem., Int. Ed.*, 2023, **62**, e202312630.
40 H. Chen, X. Cao, P. Wang, F. Huang, Y. Zhang, H. Liang, X. Bi, T. He, W. Feng, Y. Guo, Z. Ma, G. Long, Z. Yao, B. Kan, C. Li, X. Wan and Y. Chen, *J. Mater. Chem. A*, 2023, **11**, 25368–25376.
41 J. Wang, H. Chen, C. Li, Y. Lin, Y. Yang, Z. Ma and Y. Lu, *Chem. Eng. J.*, 2023, 477.
42 K. Liu, Y. Jiang, F. Liu, G. Ran, F. Huang, W. Wang, W. Zhang, C. Zhang, J. Hou and X. Zhu, *Adv. Mater.*, 2023, **35**, 2300363.
43 H. Chen, Y. Zou, H. Liang, T. He, X. Xu, Y. Zhang, Z. Ma, J. Wang, M. Zhang, Q. Li, C. Li, G. Long, X. Wan, Z. Yao and Y. Chen, *Sci. China: Chem.*, 2022, **65**, 1362–1373.
44 Y. Zhao, H. Chen, C. Zhu, J. Yuan, Y. Li, J. Hai, Y. Hu, L. Jiang, G. Chen and Y. Zou, *Mater. Chem. Front.*, 2020, **4**, 3310–3318.
45 Z. Chen, J. Ge, Y. Guo, M. Zhao, J. Shi, Y. Qiu, E. Zhou and Z. Ge, *ACS Energy Lett.*, 2022, **7**, 3432–3438.
46 D. Qiu, J. Zhang, K. Lu and Z. Wei, *Nano Res.*, 2023, **16**, 11630–11637.
47 L. Zhang, K. Yang, D. Qiu, J. Zhang, Z. Wei and K. Lu, *Chem. Eng. J.*, 2024, **481**, 148648.
48 Y. Ding, S. Xiong, M. Li, M. Pu, Y. Zhu, X. Lai, Y. Wang, D. Qiu, H. Lai and F. He, *Small*, 2023, 2309169, DOI: 10.1002/smll.202309169.
49 X. Si, Y. Huang, W. Shi, R. Wang, K. Ma, Y. Zhang, S. Wu, Z. Yao, C. Li, X. Wan and Y. Chen, *Adv. Funct. Mater.*, 2023, **33**, 2306471.
50 T. Duan, W. Feng, Y. Li, Z. Li, Z. Zhang, H. Liang, H. Chen, C. Zhong, S. Jeong, C. Yang, S. Chen, S. Lu, O. A. Rakitin, C. Li, X. Wan, B. Kan and Y. Chen, *Angew. Chem., Int. Ed.*, 2023, **62**, e202308832.
51 T. Xu, Z. Luo, R. Ma, Z. Chen, T. A. Dela Pena, H. Liu, Q. Wei, M. Li, C. Zhang, J. Wu, X. Lu, G. Li and C. Yang, *Angew. Chem., Int. Ed.*, 2023, **62**, e202304127.
52 W. Wei, C. Zhang, Z. Chen, W. Chen, G. Ran, G. Pan, W. Zhang, P. Muller-Buschbaum, Z. Bo, C. Yang and Z. Luo, *Angew Chem. Int. Ed. Engl.*, 2024, **63**, e202315625.
53 X. Ran, Y. Shi, D. Qiu, J. Zhang, K. Lu and Z. Wei, *Nanoscale*, 2023, **15**, 18291–18299.
54 L. Zhang, Z. Zhang, D. Deng, H. Zhou, J. Zhang and Z. Wei, *Adv. Sci.*, 2022, **9**, e2202513.
55 J.-W. Lee, C. Sun, C. Lee, Z. Tan, T. N.-L. Phan, H. Jeon, D. Jeong, S.-K. Kwon, Y.-H. Kim and B. J. Kim, *ACS Energy Lett.*, 2023, **8**, 1344–1353.
56 H. Zhuo, X. Li, J. Zhang, S. Qin, J. Guo, R. Zhou, X. Jiang, X. Wu, Z. Chen, J. Li, L. Meng and Y. Li, *Angew. Chem., Int. Ed.*, 2023, **62**, e202303551.
57 J. Wu, Z. Ling, L. R. Franco, S. Y. Jeong, Z. Genene, J. Mena, S. Chen, C. Chen, C. M. Araujo, C. F. N. Marchiori, J. Kimpel, X. Chang, F. H. Isikgor, Q. Chen, H. Faber, Y. Han, F. Laquai, M. Zhang, H. Y. Woo, D. Yu, T. D. Anthopoulos and E. Wang, *Angew. Chem., Int. Ed.*, 2023, **62**, e202302888.
58 M. Lv, Q. Wang, J. Zhang, Y. Wang, Z. G. Zhang, T. Wang, H. Zhang, K. Lu, Z. Wei and D. Deng, *Adv. Mater.*, 2023, **36**, 2310046.
59 H. Chen, Z. Zhang, P. Wang, Y. Zhang, K. Ma, Y. Lin, T. Duan, T. He, Z. Ma, G. Long, C. Li, B. Kan, Z. Yao, X. Wan and Y. Chen, *Energy Environ. Sci.*, 2023, **16**, 1773–1782.
60 H. Chen, B. Kan, P. Wang, W. Feng, L. Li, S. Zhang, T. Chen, Y. Yang, T. Duan, Z. Yao, C. Li, X. Wan and Y. Chen, *Angew. Chem., Int. Ed.*, 2023, **62**, e202307962.
61 T. Zhang, Y. Xu, H. Yao, J. Zhang, P. Bi, Z. Chen, J. Wang, Y. Cui, L. Ma, K. Xian, Z. Li, X. Hao, Z. Wei and J. Hou, *Energy Environ. Sci.*, 2023, **16**, 1581–1589.
62 R. Zeng, L. Zhu, M. Zhang, W. Zhong, G. Zhou, J. Zhuang, T. Hao, Z. Zhou, L. Zhou, N. Hartmann, X. Xue, H. Jing, F. Han, Y. Bai, H. Wu, Z. Tang, Y. Zou, H. Zhu, C. C. Chen, Y. Zhang and F. Liu, *Nat. Commun.*, 2023, **14**, 4148.
63 Z. G. Zhang, Y. Yang, J. Yao, L. Xue, S. Chen, X. Li, W. Morrison, C. Yang and Y. Li, *Angew. Chem., Int. Ed.*, 2017, **56**, 13503–13507.

© 2024 The Author(s). Published by the Royal Society of Chemistry

Open Access Article. Published on 07 maggio 2024. Downloaded on 18/04/2026 16:34:18.
This article is licensed under a Creative Commons Attribution-NonCommercial 3.0 Unported Licence.

64 D. Qiu, H. Zhang, C. Tian, J. Zhang, L. Zhu, Z. Wei and K. Lu, *Adv. Mater.*, 2023, **35**, 2307398.
65 Z. Zhang, Z. Li, P. Wang, H. Chen, K. Ma, Y. Zhang, T. Duan, C. Li, Z. Yao, B. Kan, X. Wan and Y. Chen, *Adv. Funct. Mater.*, 2023, **33**, 2214248.
66 Z. Zhang, Z. Li, B. Kan, T. Chen, Y. Zhang, P. Wang, Z. Yao, C. Li, B. Zhao, M. Li, T. Duan, X. Wan and Y. Chen, *Nano Energy*, 2023, **116**, 108766.
67 Y. Huang, X. Si, R. Wang, K. Ma, W. Shi, C. Jiang, Y. Lu, C. Li, X. Wan and Y. Chen, *J. Mater. Chem. A*, 2023, **11**, 14768–14775.
68 F. Liu, L. Zhou, W. Liu, Z. Zhou, Q. Yue, W. Zheng, R. Sun, W. Liu, S. Xu, H. Fan, L. Feng, Y. Yi, W. Zhang and X. Zhu, *Adv. Mater.*, 2021, **33**, 2100830.
69 M. Wang, Y. Shi, Z. Zhang, Y. Shen, M. Lv, Y. Yan, H. Zhou, J. Zhang, K. Lv, Y. Zhang, H. Peng and Z. Wei, *Nanoscale Horiz.*, 2023, **8**, 1073–1081.
70 H. Liu, Z. Chen, R. Peng, Y. Qiu, J. Shi, J. Zhu, Y. Meng, Z. Tang, J. Zhang, F. Chen and Z. Ge, *Chem. Eng. J.*, 2023, **474**, 145807.
71 Z. Chen, J. Zhu, D. Yang, W. Song, J. Shi, J. Ge, Y. Guo, X. Tong, F. Chen and Z. Ge, *Energy Environ. Sci.*, 2023, **16**, 3119–3127.
72 Y. F. Shen, H. Zhang, J. Zhang, C. Tian, Y. Shi, D. Qiu, Z. Zhang, K. Lu and Z. Wei, *Adv. Mater.*, 2023, **35**, 2209030.

© 2024 The Author(s). Published by the Royal Society of Chemistry